arXiv:1510.06256v3 [cond-mat.mtrl-sci] 28 Jan 2016

Titanium Nitride as a Seed Layer for Heusler Compounds

Alessia Niesen,* Manuel Glas, Jana Ludwig, Jan-Michael Schmalhorst, and Günter Reiss
Center for Spinelectronic Materials and Devices, Bielefeld University, Germany

Roshnee Sahoo and Daniel Ebke
Max Planck Institute for Chemical Physics of Solids, Dresden, Germany

Elke Arenholz
Advanced Light Source, Lawrence Berkeley National Laboratory, Berkeley, California 94720, USA

(Dated: January 29, 2016)

Titanium nitride (TiN) shows low resistivity at room temperature (27 µΩ cm), high thermal stability and thus has the potential to serve as seed layer in magnetic tunnel junctions. High quality TiN thin films with regard to the crystallographic and electrical properties were grown and characterized by x-ray diffraction and 4-terminal transport measurements. Element specific x-ray absorption spectroscopy revealed pure TiN inside the thin films. To investigate the influence of a TiN seed layer on a ferro(i)magnetic bottom electrode in magnetic tunnel junctions, an out-of-plane magnetized $Mn_{2.45}Ga$ as well as in- and out-of-plane magnetized Co_2FeAl thin films were deposited on a TiN buffer, respectively. The magnetic properties were investigated using a superconducting quantum interference device (SQUID) and anomalous Hall effect (AHE) for $Mn_{2.45}Ga$. Magneto optical Kerr effect (MOKE) measurements were carried out to investigate the magnetic properties of Co_2FeAl. TiN buffered $Mn_{2.45}Ga$ thin films showed higher coercivity and squareness ratio compared to unbuffered samples. The Heusler compound Co_2FeAl showed already good crystallinity when grown at room temperature on a TiN seed-layer.

I. INTRODUCTION

Spintronic exploits the influence of the electron's spin on its transport in solids. The key component of spintronic applications, like magnetic sensors or storage media, is the magnetic tunnel junction (MTJ). Spin dependent transport phenomena in MTJ's, called tunnel magnetoresistance (TMR) effect, could be maximized for materials with high spin polarization. Thus half-metallic materials are preferred, due to a spin polarization of 100 % at the Fermi level. The half-metallic characteristic has been predicted for oxide compounds like Fe_3O_4 (Magnetite) and several Heusler compounds.[1,2] To achieve high crystalline ordering of the thin films, the lattice mismatch between the material and the substrate or seed layer has to be minimized. In addition a metallic buffer layer could act as a conduction layer. Common seed layers for Heusler compounds are Cr ($a_{Cr} = 2.88$ Å) and Pt ($a_{Pt} = 3.92$ Å). Co-based Heusler compounds, like Co_2FeAl (CFA), Co_2FeSi (CFS), or Co_2MnSi (CMS) have a lattice constant of $a_{Heusler} \approx 5.7$ Å. Therefore the use of a Cr buffer or MgO substrate leads to epitaxial growth.[3] To maintain the thermal stability at shrinking device sizes, an out-of-plane oriented magnetization of the material is advantageous. Therefore perpendicularly magnetized $Mn_{3-x}Ga$ ($0.15 \leq x \leq 2$) compound found recently a lot of interest. The perpendicular magnetocrystalline anisotropy (PMA) of the binary Mn-Ga compound is an intrinsic effect based on a crystal anisotropy. The spin polarization at the Fermi level of Mn-Ga is predicted to be 88 % for the tetragonally distorted phase.[4] This crystalographic phase is formed if the mismatch between substrate and the thin film is small. In addition, the transition from the cubic $D0_3$ into the tetragonal $D0_{22}$ phase takes place at temperatures above 500°C.[5] To increase the applicability of these materials in magnetic tunnel junctions an optimized buffer layer is needed. Pt is a promising material, due to the in-plane lattice constant of 3.92 Å and a lattice mismatch of 0.2 % to the in-plane lattice constant of the tetragonally distorted Mn-Ga ($D0_{22}$). Unfortunatly the favored growth direction of Pt on MgO (100) and $SrTiO_3$ (100) substrates is the (111) direction. Crystalline growth in the (001) direction is achieved by complicated preparation techniques. Furthermore Pt is a critical raw material compared to Cr or Ti. For 45 degree rotated growth of the Mn-Ga the lattice mismatch with Cr is 5 %. Several groups reported crystalline Mn-Ga thin films on Cr buffered MgO substrates. The diffusion temperature of Cr, however, is around 450°C, while Mn-Ga requires a deposition temperature of around 550°C. The diffusion problem also lowers the applicability of a Cr buffer for the Co-based Heusler compounds, like Co_2FeAl, Co_2FeSi and Co_2MnSi. To achieve high crystalline order of these compounds ($L2_1$ crystal structure) post-annealing processes have to be carried out at temperatures around 500 °C. Investigations showed decreased TMR after the post annealing at such high temperatures, explained by Cr diffusion into the ferromagnetic electrode.[3,6] Due to the high thermal stability (melting point 2950 °C)[7] interdiffusion of TiN is prevented. Another advantage is the low electrical resistivity of sputter deposited TiN (16 µΩ cm) and a surface roughness below 1 nm.[8,9] The lattice constant of TiN (fcc structure) is 4.24 Å and therefore suitable for various Heusler compounds. By rotating the unit cell of the Co-based Heusler compounds by 45 degree a lattice

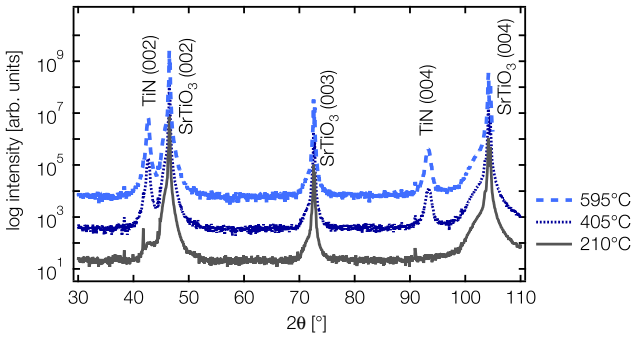

FIG. 1. X-ray diffraction pattern for DC sputter deposited TiN thin films (30 nm) on $SrTiO_3$ substrates at 210 °C, 405 °C and 595 °C.

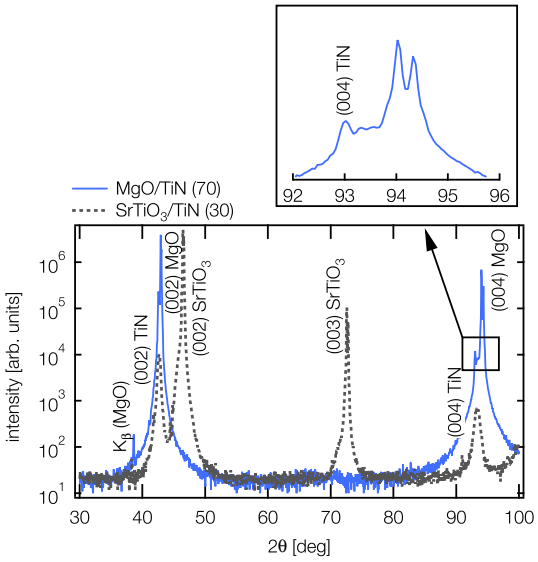

FIG. 2. X-ray diffraction pattern for TiN thin films (thickness is given in parenthesis) on MgO (blue) and $SrTiO_3$ (grey dashed) substrate. The cutout on top shows Laue oscillations around the (004) TiN peak.

mismatch of about 5 % is achieved.

We investigated the structural properties of sputter deposited TiN on single crystalline MgO (001) and $SrTiO_3$ (001) substrates at different deposition temperatures using x-ray diffraction (XRD) and reflection (XRR). Since the surface properties are of large significancy for applications, atomic force microscopy (AFM) was carried out to verify the surface roughness. Temperature dependent transport measurements were realized in a closed cycled helium cryostat, with a temperature range from 2 K to 300 K. X-ray absorption spectroscopy (XAS) was performed at beamline (BL) 6.3.1 of the Advanced Light Source in Berkeley. The Nitrogen K-edge and Titanium L-edges were investigated by surface sensitive total electron yield (TEY) and bulk sensitive luminescence mode (LM) in normal incidence. Furthermore, we investigated the crystallographic and magnetic properties of Co_2FeAl and $Mn_{3-x}Ga$ with TiN seed layer deposited on MgO and $SrTiO_3$ substrates.

II. EXPERIMENTAL

DC and RF magnetron sputtering was used to prepare the samples. The TiN as well as the $Mn_{2.45}Ga$ layers were deposited in an UHV sputtering system with a base pressure below 3×10^{-9} mbar. Reactive sputtering in an Argon - Nitrogen atmosphere results in stoichiometric Ti_1N_1 thin films. During the sputtering a N flow of 2 sccm combined with 20 sccm Ar was used, leading to a deposition pressure of 1.6×10^{-3} mbar. Because of the low lattice mismatch with TiN (below 0.7 %) MgO (100) single crystalline substrates were used. $SrTiO_3$ (100) substrates were utilized, due to the low mismatch with the Mn-Ga crystal (below 1 %). A $Mn_{60}Ga_{40}$ composite target and an Ar pressure of 1.7×10^{-3} mbar were used to deposit the $Mn_{2.45}Ga$ thin films on top of the TiN. The deposition temperature T_{dep} of TiN was 210 °C, 405 °C, 595 °C and 830 °C, respectively. Whereas the Mn-Ga was deposited at 550 °C and 595 °C. In addition TiN buffered Co_2FeAl thin films on MgO and $SrTiO_3$ substrates were prepared. For the Co_2FeAl, the substrates with a TiN buffer layer were transfered to another magnetron sputtering machine, without vacuum break. Here the base pressure was 1×10^{-7} mbar. Stoichiometric Co_2FeAl was deposited from a composite target under an Ar pressure of 2.3×10^{-3} mbar. On top of the Heusler compound a 2 nm thick MgO layer was deposited to protect the stack from degradation.

III. RESULTS

A. Chrystallographic, structural and electrical properties of the TiN seed-layer

Crystallographic properties of the TiN thin films (30 nm) were determined using an X'Pert Pro diffractometer (Cu anode). The TiN films showed no dependence of their crystalline quality on the deposition temperature on MgO substrates. Even at 210 °C an epitaxial growth was obtained (not shown). On the contrary, TiN layers on $SrTiO_3$ required a deposition temperature higher than 210 °C to achieve epitaxial growth (Figure 1). Figure 2 shows an XRD pattern comparison of TiN deposited on MgO and $SrTiO_3$ substrate at 405 °C. The 70 nm thick TiN film deposited on MgO shows Laue oscillations, which are a clear evidence for high crystalline coherence (cutout in Figure 2). Due to the low lattice mismatch with MgO the TiN film reflexes are close to the substrate peaks and therefore difficult to investigate. The out-of-plane lattice constant, determined by the shoulder

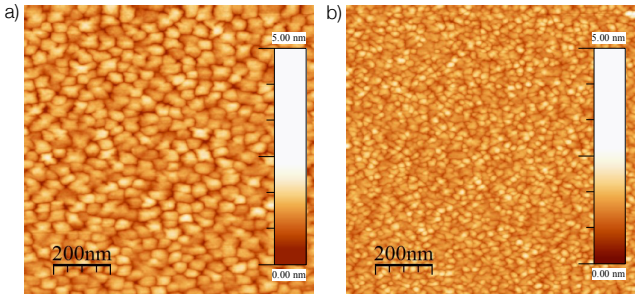

FIG. 3. Atomic force microscopy images (1 µm^2 section) of TiN thin films deposited at 595 °C on a) MgO and b) $SrTiO_3$ substrates. The grain size on $SrTiO_3$ substrate is 25 ± 5 nm compared to 50 ± 5 nm on MgO.

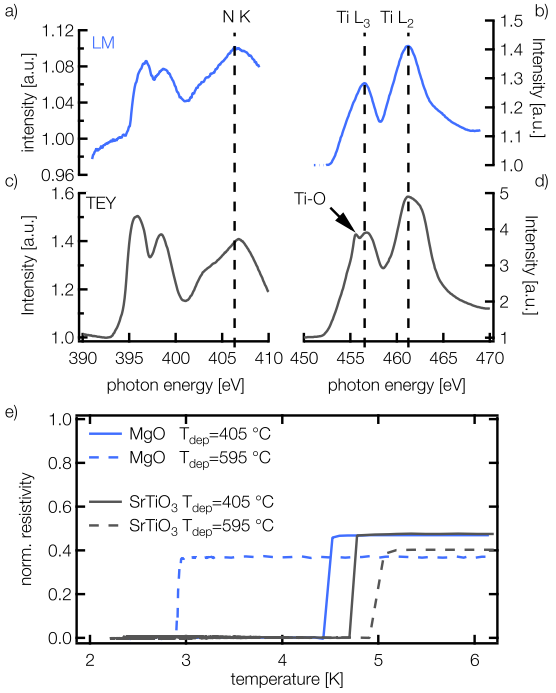

FIG. 4. X-ray absorption spectra of a) and c) N and b) and d) Ti taken in total electron yield (grey) and luminescence mode (blue). The sample was deposited at 405 °C on MgO substrate. e) Temperature dependence of the resistivity down to 2 K for TiN thin films deposited at 405 °C and 595 °C.

next to the (002) and (004) MgO reflex, is $c = 4.25$ Å. On $SrTiO_3$ substrates, the reflexes of the TiN layer are clearly visible and exhibit the same out-of-plane lattice constant. Atomic force microscopy and x-ray reflection measurements were carried out to investigate the surface roughness of the TiN layers. The roughness obtained by XRR is between 0.6 nm and 1 nm for all samples. The lowest value of 0.6 ± 0.1 nm was obtained for DC deposited TiN with a deposition temperature of 595 °C on both substrate types. AFM measurements of this samples (on a 3 µm^2 section) showed an RMS (root mean square) value of 0.2 nm on MgO (Figure 3 a) and 0.5 nm on $SrTiO_3$ (Figure 3 b) substrate. The lower roughness values determined by AFM are attributed to the smaller scanned section compared to the XRR measurements. Another reason is that the AFM is only sensitive to the surface, so that possible gaps between the grains could not be detected. Whereas x-rays are penetrating into the sample surface and therefore are sensitive to steep grain boundaries. However, on $SrTiO_3$ both values are in good agreement, which was attributed to the smaller grain size of 25 ± 5 nm compared to 50 ± 5 nm on MgO. Due to the reduced lateral grain size we obtain more grain boundaries on the scanned 3 µm^2 section, which leads to increased roughness.

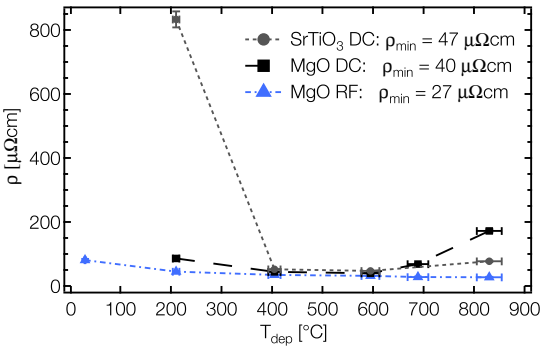

FIG. 5. Resistivity dependence (measured at room temperature) of TiN on the deposition temperature T_{dep} and the substrate. The high resistivity value for TiN deposited on $SrTiO_3$ at 210 °C confirms that there is no crystalline growth.

T_{dep} (°C)	on MgO (100)	on STO (100)
405	4.65 K	4.78 K
595	2.94 K	5 K

TABLE I. Dependence of the transition temperature into the superconducting state of sputter deposited TiN on the substrate and the deposition temperature.

The chemical properties of TiN thin films were investigated using XAS. Figure 4 a) - d) depicts the X-ray absorption spectra of N and Ti taken in total electron yield TEY (grey) and luminescence mode LM (blue). The weak multiplet structure of the L_3-Ti-edge indicates a small amount of Ti-O on the surface. However, the bulk sensitive LM spectra of Ti and N are in good agreement with the literature.[10]

Temperature dependent transport measurements in a closed cycled He-cryostat revealed a transition into the superconducting state. The transition temperature T_C showed a dependence on the substrate as well as on the deposition temperature of TiN (Table I and Figure 4 e). The highest T_C of 5 K was achieved for TiN deposited at 595 °C on $SrTiO_3$ substrate. However, the same stack on MgO revealed the lowest T_C of 2.94 K. Transport measurements at room temperature also showed a de-

position temperature dependence of the resistivity (Figure 5). The lowest values of 27 µΩ cm (47 µΩ cm) for RF deposited TiN on MgO (DC deposited on $SrTiO_3$) was found for deposition temperatures of 830 °C (595 °C). These data are in good agreement with the one reported by Shin et al.[11] The high resistivity value of 833 µΩ cm for TiN deposited at 210 °C (Figure 5) confirms the assumption that this temperature is too low to achieve crystalline growth of TiN. The temperature and substrate dependence of the resistivity was attributed to the different grain sizes and film quality of TiN obtained by different sputtering condicions. Due to the lower grain sizes on $SrTiO_3$ there are more grain boundaries inside the TiN films and therefore more perturbations, which leads to a decreased conductance of the layer. Then again, this sample showed the highest transition temperature into the superconducting state, which is an evidence for high film quality with a low amount of impurities inside the layer. On the other hand, we obtained a reverse behavior for samples on MgO. The low resistivity of the on MgO substrates deposited thin films is attributed to bigger grains and high film quality of the TiN compared to samples on $SrTiO_3$. In this case, increasing the deposition temperature leads to reduced T_C. This reduction could be caused by oxygen impurities inside the TiN.[12] Increasing the deposition temperature causes a diffusion of oxygen atoms from the MgO substrate into the TiN layer leading to the formation of a Ti-O interlayer between the substrate and the TiN. Ti-O is a semiconductor and therefore even a small amount inside the thin TiN layer disturbes the transition into the superconducting state.

B. TiN buffered $D0_{22}$-Mn-Ga thin films

To investigate the suitability of TiN as a seed layer, we deposited two different Heusler compounds on top of the TiN. In a first attempt a perpendicularly magnetized $Mn_{2.45(6)}Ga$ (25 nm) thin film was deposited on a 30 nm TiN buffer layer on MgO and $SrTiO_3$ substrates. The TiN seed-layer (30 nm thickness) was DC sputter deposited at deposition temperatures of 405 °C, 595 °C and 830 °C, respectively. The Mn-Ga was deposited at 550 °C in order to achieve the tetragonally distorted $D0_{22}$ structure.[13] For all TiN deposition temperatures the Mn-Ga shows two phases, a mixture of the tetragonal $D0_{22}$ structure with predicted out-of-plane magnetization and the cubic $D0_3$ phase with predicted in-plane magnetization (Figure 6 a). However, for TiN deposited at 830 °C a maximum amount of the $D0_{22}$ phase was observed. Furthermore, we added a Mn-Ga thin film on $SrTiO_3$ substrate without a TiN buffer layer for comparison. The optimal deposition temperature to achieve the $D0_{22}$ structure of the $Mn_{2.45}Ga$ without a buffer layer was 595 °C and therefore higher in contrast to TiN buffered samples. All samples show the fundamental (004) $D0_{22}$-Mn-Ga reflex, corresponding

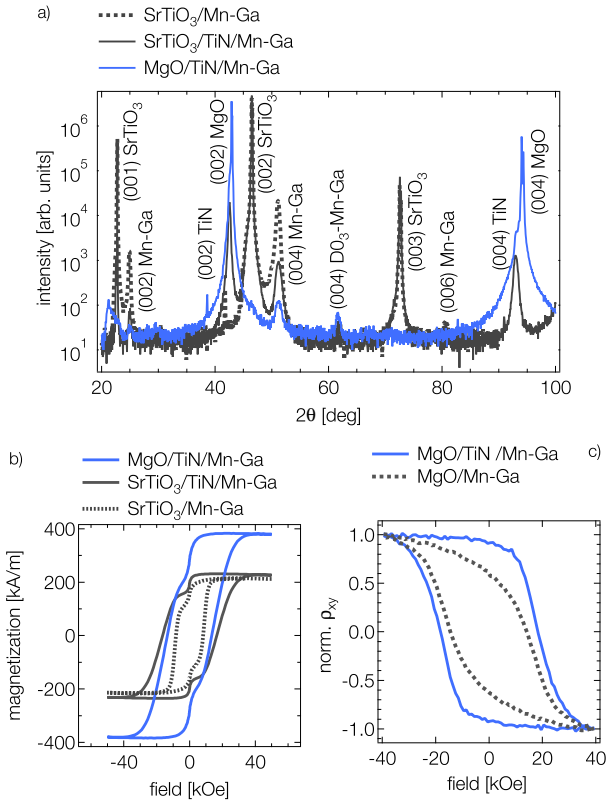

FIG. 6. a) XRD pattern of a $Mn_{2.45}Ga$ thin film with TiN seed layer on MgO (blue) and $SrTiO_3$ (grey) substrate. The deposition temperature was 550 °C for the Mn-Ga thin film and 830 °C for the TiN. For comparison a plain $Mn_{2.45}Ga$ thin film on $SrTiO_3$ substrate is added (grey dashed), whereas the deposition temperature was 595 °C. The Mn-Ga layer thickness was 25 nm for each sample. b) SQUID and c) AHE hysteresis loops of $Mn_{2.45}Ga$ thin films with TiN seed layer on MgO (blue) and $SrTiO_3$ (grey) substrate. The deposition temperature of the Mn-Ga was 550 °C and 830 °C for the TiN buffer. For comparison a plain $Mn_{2.45}Ga$ thin film on $SrTiO_3$ and MgO deposited at 595 °C is depicted (grey dashed).

to $c_{D0_{22}}$ = 7.15 Å without TiN buffer and 7.14 Å with TiN buffer. The lattice mismatch with the TiN buffer leads to an expansion of the Mn-Ga unit cell along the *a*-*b* plane, which results in a lower *c* lattice constant. Further to the fundamental $D0_{22}$ peak, the superlattice (002) reflex is visible for all samples. However, the superlattice (006) peak is only visible for Mn-Ga thin films without TiN buffer. This indicates a lower amount and crystallinity of the tetragonally distorted $D0_{22}$ phase on TiN buffered samples. The fundamental (004) peak of the $D0_3$ phase is weakly distinct, corresponding to c_{D0_3} = 5.99 Å on $SrTiO_3$ and c_{D0_3} = 6.02 Å on MgO. The magnetic properties of Mn-Ga were investigated using a superconducting quantum interference device. Figure 6 b) depicts the magnetization *M* of TiN buffered Mn-Ga thin films on MgO (blue) and $SrTiO_3$ (grey). For comparison an unbuffered Mn-Ga thin film (grey

dashed) is shown. An overview of the coercivity H_c and the squareness S_R of TiN buffered Mn-Ga films on MgO and $SrTiO_3$ is given in Table II. We defined the squareness ratio by $M(0\,\mathrm{kOe})/M(60\,\mathrm{kOe})$ for the SQUID measurements. TiN buffered $Mn_{2.45}Ga$ shows increased coercivity and squareness on both substrate types. To prove this effect, additionally AHE measurements were carried out. Figure 6 c) shows normalized out-of-plane AHE hysteresis curves for TiN buffered (blue) and unbuffered Mn-Ga layers (grey dashed). The H_c and S_R values are given in Table II. In this case we also observe an enhancement of the coercive field and squareness ratio for the TiN buffered layer. The squareness ratio is defined by $\rho_{xy}(0\,\mathrm{kOe})/\rho_{xy}(40\,\mathrm{kOe})$. It reveals a stronger enhancement compared to the sample on $SrTiO_3$ and increases from a value of 0.62 ± 0.05 to 0.90 ± 0.05. TiN buffered Mn-Ga thus requires lower deposition temperature compared to unbuffered samples to achieve an out-of-plane magnetization with high coercivity and squareness ratio. The saturation magnetization of 400 kA/m on MgO and 200 kA/m on $SrTiO_3$ is in good agreement with the peviously reported results.[13] Interestingly, the saturation magnetization of the samples grown on MgO, is twice as high as for the samples on $SrTiO_3$. This behavior was also observed for unbuffered samples and attributed to lower crystallinity due to bigger expansion in the *a*-*b* plane for Mn-Ga on MgO substrates.[13] Obviously a 30 nm TiN layer does not change this behavior. Due to this expansion and therefore the imperfections in the crystal structure, the magnetic moments of the Mn atoms occupying the Wyckoff positons 2*b* and 4*d* are not compensating each other and this leads to an increase of the magnetization. The observed feature in the SQUID measurements around 0 kOe field (Figure 6 b) is attributed to a second phase (soft magnetic) inside the Mn-Ga crystal structure, which has a different coercive field. The soft magnetic phase dominates at low field values and therefore leads to a sudden decrease or increase of the magnetization. A similar behavior was already observed for the ternary compounds Mn-Co-Ga and Mn-Fe-Ga.[14,15]

SQUID measurements		
sample	H_c (kOe)	S_R
STO/ $Mn_{2.45}Ga$	8 ± 0.5	0.74 ± 0.05
STO/TiN/$Mn_{2.45}Ga$	16 ± 0.5	0.86 ± 0.05
MgO/TiN/$Mn_{2.45}Ga$	13 ± 0.5	0.75 ± 0.05
AHE measurements		
sample	H_c (kOe)	S_R
MgO/$Mn_{2.45}Ga$	13 ± 0.5	0.62 ± 0.05
MgO/TiN/$Mn_{2.45}Ga$	18 ± 0.5	0.90 ± 0.05

TABLE II. Coercive fields and squareness ratios of TiN buffered Mn-Ga. The TiN seed-layer (30 nm) was DC sputter deposited at 830 °C. TiN buffered Mn-Ga was deposited at 550 °C, the unbuffered Mn-Ga thin film was deposited at 595 °C.

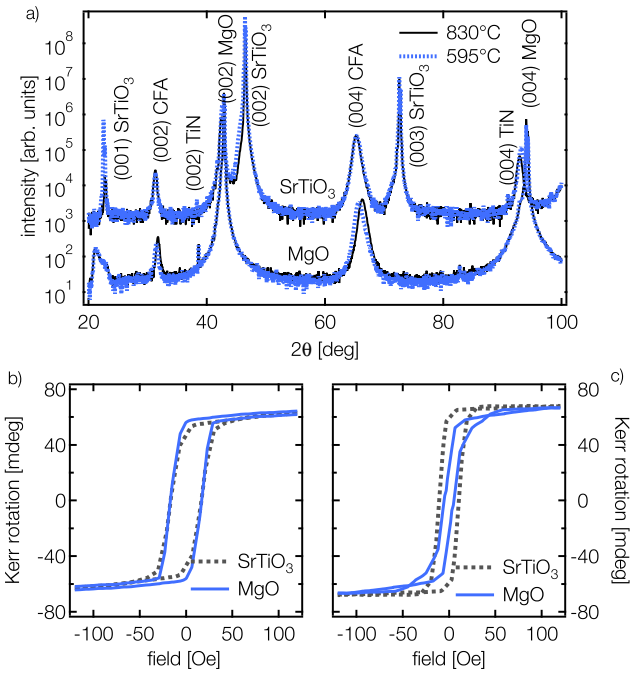

FIG. 7. a) XRD pattern of 20 nm thick Co_2FeAl films on TiN buffer deposited on MgO and $SrTiO_3$ substrates. The 30 nm thick TiN layers were deposited at 595 °C and 830 °C, respectively. b) Linear MOKE measurements of TiN buffered Co_2FeAl thin films with a TiN deposition temperature of 595 °C and c) of 830 °C on MgO (blue) and $SrTiO_3$ (grey dashed) substrates.

C. TiN buffered Co_2FeAl thin films

The influence of a TiN buffer layer on the magnetic and crystallographic properties of Co_2FeAl thin films was investigated in a second step. 20 nm and 0.9 nm thin Co_2FeAl layers were sputter deposited on a 30 nm thick TiN buffer on MgO and $SrTiO_3$ substrates. The TiN was DC sputter deposited at different temperatures (405 °C, 595 °C and 830 °C), whereas the Co_2FeAl deposition was carried out at room temperature. Figure 7 a) shows the obtained XRD spectra. Besides the characteristic TiN reflexes, the fundamental and the superlattice peak of the Co_2FeAl are clearly visible. Even in the as deposited state, the XRD scan reveals a cubic structure with a (002) superlattice peak at 31.3 degree and a fundamental (004) reflex at 65.3 degree. Therefore a B2 order of the Co_2FeAl is proofed with an out-of-plane lattice constant of 5.66 Å for MgO substrates and 5.72 Å for $SrTiO_3$ substrates. Interestingly, the lattice constant for samples on $SrTiO_3$ substrates is closer to the literature value of 5.73 Å.[16] The TiN deposition temperature does not influence the crystalline quality of the Co_2FeAl thin films.

In this case MOKE measurements were carried out to determine the magnetic properties. Figure 7 b) and c)

T_{dep}	substrate	H_c (Oe)	S_R
595 °C	MgO	17 ± 0.5	0.8 ± 0.05
	STO	17 ± 0.5	0.65 ± 0.05
830 °C	MgO	7 ± 0.5	0.2 ± 0.05
	STO	10 ± 0.5	0.87 ± 0.05

TABLE III. Coercive fields and squareness ratios of TiN buffered Co_2FeAl thin films (20 nm) with ip oriented easy magnetization axis.

T_{pa}	H_c (Oe) on MgO	H_c (Oe) on STO
360 °C	76 ± 0.3	22 ± 0.3
480 °C	329 ± 0.3	137 ± 0.1

TABLE IV. Coercive fields of TiN buffered 0.9 nm thin Co_2FeAl layers with oop oriented easy magnetization axis. The squareness ratio is 1 for each sample. The TiN seed-layer was DC sputter deposited at 405 °C.

illustrates the in-plane hysteresis loops for TiN buffered 20 nm thick Co_2FeAl films with a TiN deposition temperature of 595 °C and 830 °C. The Co_2FeAl films reveal sharp switching behavior and in-plane oriented easy magnetization axis, even in the as deposited state. The coercivity and squareness values of Co_2FeAl on TiN are shown in Table III. The squareness ratio is defined as Kerr rotation at 0 Oe divided by Kerr rotation at 150 Oe. The magnetic properties show a dependence on the substrate type as well as on the TiN deposition temperature. With increasing TiN deposition temperature, the coercive field decreases. In contrast the squareness ratio for samples on $SrTiO_3$ increases with increasing TiN deposition temperature. As previously mentioned, different deposition temperatures affect the TiN seed layer. The temperature during sputtering, and thus the surface energy has a strong influence on the crystal structure and grain size of the material. Structural changes of TiN obviously influence the on top deposited material. Especially the grain sizes of the thin Co_2FeAl layers adjust to the grain structure of the seed layer. The coherence between grain size and coercivity of nanocrystalline ferromagnets was investigated by G. Herzer.[17] He found a D^6 dependence of the coercivity for small grain sizes (up to 50 nm) and a $1/D$ dependence for bigger grains. In our case the grain size of Co_2FeAl is between 25 nm and 50 nm. Therefore, the decrease of the coercive field of Co_2FeAl could be explained by a decrease of the grain sizes.

Out-of-plane MOKE measurements for 0.9 nm thin, TiN buffered, Co_2FeAl layers (Figure 8) revealed sharp switching (squareness ratio = 1) and high thermal stability for both substrate types. Even for post annealing temperatures T_{pa} around 500 °C strong perpendicular magnetic anisotropy and an increase of the coercivity was observed. The coercivity of the Co_2FeAl thin layers post annealed at 360 °C is 76 ± 0.3 Oe on MgO (blue curves) and 22 ± 0.3 Oe on $SrTiO_3$ (grey curves). Post annealing at 480 °C leads to a H_c of 329 ± 0.3 Oe on MgO

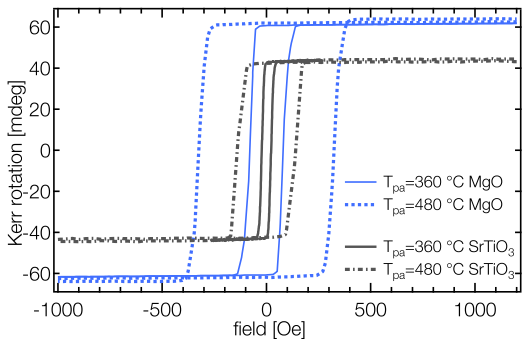

FIG. 8. Perpendicular MOKE hysteresis loops of TiN (30)/Co_2FeAl (0.9)/MgO (2) layer systems post annealed at different temperatures (film thicknesses are given in parenthesis). The TiN seed-layer was DC sputter deposited at 405 °C. High PMA and an increase of the coercive field was observed with increasing post annealing temperature.

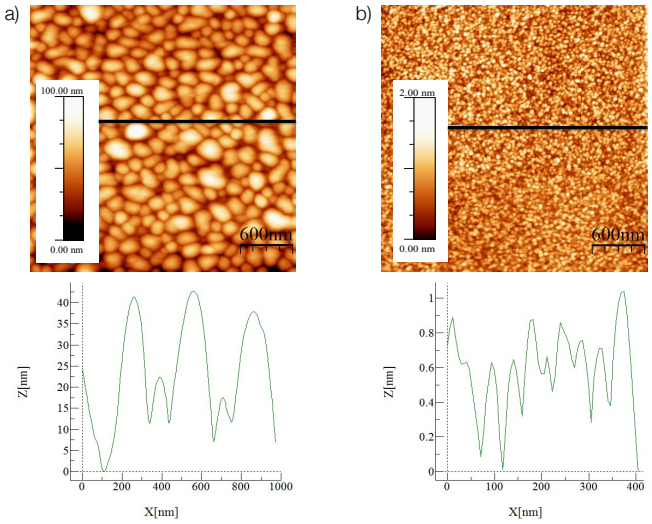

FIG. 9. AFM images (3 µm^2 section) of TiN buffered a) $Mn_{2.45}Ga$ thin film (25 nm) deposited at 550 °C and b) Co_2FeAl thin film (10 nm) deposited at room temperature. The graphs below show the profiles of the sample surface at the marked position (black line).

and 137 ± 0.1 Oe on $SrTiO_3$. An overview is also given in Table IV. Compared to the results of Wen et al.[18] for Pt buffered Co_2FeAl thin films, where the PMA vanishes for post annealing temperatures of 400 °C, the TiN buffered Co_2FeAl layers provide high thermal stability, which in turn is beneficial for applications. Additionally the Co_2FeAl shows a dependence of the coercivity on the used substrate. We also attribute this behavior to different grain sizes of TiN on MgO ($SrTiO_3$) substrates. As already shown in Figure 3 the grain size of TiN on MgO is twice as high (50 nm) as on $SrTiO_3$ (25 nm). For the as deposited state we get a good agreement with a D^3 proportionality between coercivity and grain size. This behavior was explained theoretically by Alben et al. who

found this proportionality for materials, where the induced anisotropy K_u exceeds the structural anisotropy K.[19] In case of Co_2FeAl this is a necessary condition to obtain the perpendicular magnetocrystalline anisotropy, which we showed by the out-of-plane hysteresis curves. (Figure 8). A detailed discussion of the structural and magnetic properties of TiN buffered Co_2FeAl thin films will be published elsewhere.

Investigations of the surface properties of the two compounds via AFM (Figure 9) revealed strong difference between the surface properties of TiN buffered $Mn_{2.45}Ga$ and Co_2FeAl. $Mn_{2.45}Ga$ showed high roughness (RMS = 16 nm) and island growth (200 nm grain size, determined using profiles of the AFM measurements (Figure 9), which is a strong drawback with regard to the applicability. However, Co_2FeAl thin films showed smooth surface (RMS = 0.25 nm), no island growth and small grains (50 nm). With regard to the integration of this layers into magnetic tunnel junctions, where low roughness plays an important role, TiN buffered Co_2FeAl is a promissing candidate.

IV. CONCLUSION

We successfully prepared (001) oriented TiN thin films on MgO and $SrTiO_3$ substrates. XAS measurements revealed the formation of pure TiN in the thin films. A transition into the superconducting state was observed below 5 K. Transport measurements at room temperature showed a resistivity of 27 µΩ cm and 47 µΩ cm on MgO and $SrTiO_3$ substrates, respectively. It has been demonstrated that out-of-plane magnetized $Mn_{2.45}Ga$ and Co_2FeAl thin films crystallize well on a TiN seed layer. Even in the as deposited state Co_2FeAl provides the B2 crystal structure. Mn-Ga thin films exhibit higher coercivity and squareness ratio when prepared on a TiN buffer. In addition a lower deposition temperature for TiN buffered systems was observed. In-plane magnetized 20 nm thick Co_2FeAl films revealed high squareness ratio even in the as prepared state. 0.9 nm thin Co_2FeAl with out-of-plane oriented easy magnetization axis showed high thermal stability for temperatures up to 500 °C. TiN provides various advantages. The low resistivity makes TiN a promising seed layer for Heusler compounds in MTJ's. Besides the low roughness, high thermal stability and conductivity, it also enhances the out-of-plane magnetocrystalline anisotropy and optimizes the switching behavior of the used Heusler material. In case of Co_2FeAl, TiN additionally enhances the thermal stability and therefore is highly preferable for applications.

ACKNOWLEDGMENTS

The authors gratefully acknowledge financial support by the Deutsche Forschungsgemeinschaft (DFG, Contract No. RE 1052/32-1) and the opportunity to work at BL 6.3.1 of the Advanced Light Source, Berkeley, USA, which is supported by the Director, Office of Science, Office of Basic Energy Sciences, of the U.S. Department of Energy under Contract No. DE-AC02-05CH11231. D.E. is financially supported by the ERC Advanced Grant (291472 Idea Heusler).

* aniesen@physik.uni-bielefeld.de

[1] J. J. Versluijs, M. A. Bari, and J. Coey, Physical Review Letters **87**, 026601 (2001).
[2] R. Degroot, F. Mueller, P. Vanengen, and K. Buschow, Physical Review Letters **50**, 2024 (1983).
[3] C. Sterwerf, M. Meinert, J.-M. Schmalhorst, and G. Reiss, IEEE Transactions on Magnetics **49**, 4386 (2013).
[4] B. Balke, G. H. Fecher, J. Winterlik, and C. Felser, Applied Physics Letters **90**, 152504 (2007).
[5] M. Glas, C. Sterwerf, J.-M. Schmalhorst, D. Ebke, C. Jenkins, E. Arenholz, and G. Reiss, Journal of Applied Physics **114**, 183910 (2013).
[6] D. Ebke, P. Thomas, O. Schebaum, M. Schäfers, D. Nissen, V. Drewello, A. Hütten, and A. Thomas, Journal of Magnetism and Magnetic Materials **322**, 996 (2010).
[7] M. Pritschow, Ph.D. thesis, Institut für Mikroelektronik Stuttgart (2007).
[8] F. Magnus, A. S. Ingason, S. Olafsson, and J. T. Gudmundsson, Thin Solid Films **520(5)**, 1621 (2011).
[9] Y. Krockenberger, S.-i. Karimoto, H. Yamamoto, and K. Semba, Journal of Applied Physics **112**, 083920 (2012).
[10] L. Soriano, M. Abbate, H. Pen, M. T. Czyżyk, and J. C. Fuggle, Journal of electron spectroscopy and related phenomena **62**, 197 (1993).
[11] C.-S. Shin, S. Rudenja, D. Gall, N. Hellgren, T.-Y. Lee, I. Petrov, and J. E. Greene, Journal of Applied Physics **95**, 356 (2004).
[12] A. Münster and K. Sagel, Zeitschrift für Physik , 139 (1956).
[13] M. Glas, D. Ebke, I. M. Imort, P. Thomas, and G. Reiss, Journal of Magnetism and Magnetic Materials **333**, 134 (2013).
[14] C. Fowley, S. Ouardi, T. Kubota, O. Yildirim, A. Neudert, K. Lenz, V. Sluka, J. Lindner, J. M. Law, S. Mizukami, G. H. Fecher, C. Felser, and A. M. Deac, Journal of Physics D: Applied Physics **48**, 164006 (2015).
[15] T. Gasi, A. K. Nayak, J. Winterlik, V. Ksenofontov, P. Adler, M. Nicklas, and C. Felser, Applied Physics Letters **102**, 202402 (2013).
[16] K. Buschow, P. G. Van Engen, and R. Jongebreur, Journal of Magnetism and Magnetic Materials **38**, 1 (1983).
[17] G. Herzer, IEEE Transactions on Magnetics **26**, 1397 (1990).
[18] Z. Wen, H. Sukegawa, S. Mitani, and K. Inomata, Applied Physics Letters **98**, 192505 (2011).
[19] R. Alben, J. Becker, and M. Chi, Journal of Applied Physics **49**, 1653 (1978).